Article:
Xiao, X, Jia, H, Pervaiz, S et al. (2020) Molten Salt/Metal Foam/Graphene Nanoparticle Phase Change Composites for Thermal Energy Storage. ACS Applied Nano Materials, 3 (6). pp. 5240-5251. ISSN: 2574-0970

https://doi.org/10.1021/acsanm.0c00648

Molten Salt/Metal Foam/Graphene Nanoparticle Phase Change Composites for Thermal Energy Storage

Xin Xiao, [*,†] Hongwei Jia, [‡] Shahid Pervaiz, [†] Dongsheng Wen [**,§,†]

[†] School of Chemical and Process Engineering, University of Leeds, Leeds LS2 9JT, UK

[‡] School of Environmental Science and Engineering, Donghua University, Shanghai 201620, China

[§] School of Aeronautic Science and Engineering, Beihang University, Beijing 100191, China

ABSTRACT: The binary and ternary mixtures of nitrates are desirable phase change materials (PCMs) as latent heat thermal energy storage media for solar energy applications. In this study, graphene oxide was synthesized with graphite powder firstly, then it was doped into HITEC salt or solar salt solvent with sonication using two-step methods. Metal foams including nickel and copper ones were impregnated with the salt seeded with graphene (nanocomposite) finally. The morphologies of the synthesized composites were analyzed extensively, while the thermo-physical properties of the composites were both theoretically predicted and experimentally investigated. The results indicated that metal foam was compatible with nanocomposite, and the thermal stabilities of the composite PCMs were good regarding the thermal cycle characteristics. The

effective thermal conductivities of the salt/graphene/metal foam composites were distinctly enhanced, while the latent heats of the present composite PCMs were smaller than that of pure salt to some extent. Furthermore, the phase change temperatures shifted slightly in the presence of porous metal foam and graphene, while the addition of graphene could compensate for the reduction of specific heats of the composite PCMs caused by metal foam. Finally, it was found that the thermal effusivities of the salt/graphene/metal foam composites were larger than those of pure salt, indicating the increments of 110~270% in solid state and 150~360% in liquid state, respectively. The fundamental information of the nanocomposites with porous media could broaden their application in thermal energy storage system.

KEYWORDS: molten salt; graphene; metal foam; morphological characteristics; thermal characterization

1. INTRODUCTION

Nowadays, renewable energy as one source of energy has drawn much attention due to the increasing environmental problems such as global warming, COx emissions, depletion of zone layer, etc. Solar energy as the clean and almost endless source of renewable energy is considered as accessibility to energy resources in most countries in the world. However, energy system integrated with solar energy is short of stability and reliability, which is caused by the intermittence and instability of solar energy, as various regions with different climates. To overcome the inevitable barriers of the imbalance between energy supply and requirement, energy storage is proposed to address the time-dependant limitation essentially [1-2]. There are three different methods for energy storage, including sensible heat storage, latent heat storage and chemical heat

storage. Among them, latent heat thermal energy storage (LHTES) can provide a much higher energy storage density with a smaller temperature variation [3-4].

Molten salts as the phase change materials (PCMs), with relatively low cost and no flammability, are widely used as the storage media of LHTES system among the temperature range of 100-500 ºC. It is difficult to directly use molten salts in real systems, as their weak thermal stability and low thermal conductivity lead to low charging/discharging rates of the LHTES system. It should be noted that many techniques related to heat transfer enhancement are adopted to improve the thermo-physical properties of PCMs, and composite PCMs have received increasing research interests. One of the effective methods is to impregnate PCMs into porous media such as graphite foam and metal foam, which can significantly increase the thermal conductivities of the PCMs [6-9]. Kholmanov et al. [6] fabricated carbon nanotube (CNT) network inside continuous ultrathin graphite foam (UGF), then impregnated erythritol into the hybrid structure of UGF-CNT. The results indicated that the thermal conductivity increased to 4.1 W $m^{-1}K^{-1}$ and the sub-cooling of erythritol was apparently suppressed. Wang et al. [7] synthesized cetyl palmitate/nickel foam composites via melting infiltration method. It was found that the thermal conductivities of the composites fabricated with nickel foam of the pore sizes of 70, 90, 110 PPI were 0.6465, 0.6942, 1.6687 W $m^{-1}K^{-1}$, respectively, compared to that of pure cetyl palmitate of 0.3432 W $m^{-1}K^{-1}$. Xiao et al. [8] synthesized the composite PCMs with paraffin and copper/nickel foams of different porosities and pore sizes under vacuum impregnation method. The highest effective thermal conductivity in the results was 16.01 W $m^{-1}K^{-1}$, which was fabricated with copper foam of 89.0% porosity and 1.0 mm pore size. Additionally, it was found that the pore size hardly affected the effective thermal conductivity of the composite PCM. Feng et al. [9] experimentally and theoretically studied the effects of the porosity and pore density of the foam on the freezing rate,

which was conducted in a water/copper foam system with unidirectional freezing. They pointed out that the pore size slightly affected the freezing rate, and the local thermal equilibrium was verified with the temperature measurements of the foam skeleton and pore. However, majority of the studies indicated that the addition of metal foam would decrease the latent heat and specific heat of the composite PCM to some extent.

In other words, nanoparticles such as Al_2O_3, SiO_2, Fe_2O_3, TiO_2, CuO, MgO and CNT are with exceptional thermal properties, and the utilization of those materials is one of the key effective methods to improve the thermo-physical properties of pure PCMs [10-11]. Moreover, nanoparticles have been recently proposed to mitigate the issue of low specific heats of molten salts, i.e., keep and increase the specific heats of the nanocomposites [12-15]. Tiznobaik et al. [12] studied the enhancements of specific heat of molten salt (Li_2CO_3:K_2CO_3=62:38) with the addition of magnesium oxide nanoparticle. It was found that a semi-solid layer of dendritic shaped phase was formed, contributing to the enhancement of the specific heats. Riazi et al. [13] experimentally investigated the effects of the morphology and dispersion of particle on the specific heat of nano-salts fabricated by solar salt and silica nanoparticle, and stable dispersion could induce the enhancement of the specific heat by 17.6%. Song et al. [14] investigated the specific heat of the nanofluids made of $Ca(NO_3)_2 \cdot 4H_2O$-KNO_3-$NaNO_3$-$LiNO_3$ and 1.0 wt.% SiO_2 nanoparticle with the size of 20 nm. The maximum specific heat increased by 17.0% when the nanofluid was prepared under the condition of 750 rpm (stirring rate) and 15 min (mixing time). An enhancement of 34.0% in the specific heat of binary carbonate salt was obtained by Zhang et al. [15], while the salt was microencapsulated with silica shell. Graphene is with large specific surface area and stable chemical characteristics, and extensively studied recently [16-23]. Yang et al. [20] synthesized the composite PCMs made of polyethylene glycol (PEG) and hybrid graphene aerogels (HGA) via

vacuum impregnation, where HGA was composited of graphene oxide (GO) and graphene nanoplatelets (GNP). It was found that the PEG/HGA composite presented high thermal conductivity and good shape stabilization, e.g., the composite (0.45 wt.% GO, 1.8 wt.% GNP) had the thermal conductivity of 1.43 W $m^{-1}K^{-1}$, while that of pure PEG was 0.31 W $m^{-1}K^{-1}$. Chen et al. [21] synthesized mePCMs with graphene oxide and octadecylamine (GO-ODA) via in-situ polymerization. It was found that the supercooling of n-octadecane could be retrieved, and the thermal conductivity and energy storage ability were substantially enhanced. Kant et al. [22] numerically investigated the melting characteristics of an aluminum square cavity, which was encapsulated with Capric Acid, $CaCl_2 \cdot 6H_2O$, or n-octadecane mixed with graphene nanoparticles in three different volumetric ratios (1%, 3%, and 5%). It was found that the graphene improved the melting characteristics, but considerably degraded its natural convection heat transfer efficiency. Yuan et al. [23] investigated the influences of the surface functionalization of graphene on the properties of the polyethylene glycol/graphene composites with MD simulations. It was found that the graphene increased the phase change temperature and specific heat. But these studies indicated that the heat transfer enhancement with the addition of nanoparticles is very limit.

The integration of metal foam and nanoparticles together to enhance the thermo-physical properties of pure salt can fill the research gap between thermal conductivity and thermal storage capacity. However, the research on doping nanoparticles into molten salt/metal foam composite is very few. The investigations of thermo-physical properties of the salt/graphene nanocomposites and salt/graphene/metal foam composites are of vital importance. Based on the research background of the storage of solar energy and geothermal energy within the temperature range of 100~300 ^{o}C for electricity generation, this research will be focused on preparation and characterization of the salt/graphene/metal foam composites so as to see how the thermo-physical

properties of pure salt are affected by additives. Considering the suitable phase change temperatures and moderate melting enthalpies [24-25], HITEC salt (40 wt.% $NaNO_2$, 7 wt.% $NaNO_3$ and 53 wt.% KNO_3) and solar salt (60 wt.% $NaNO_3$ and 40 wt.% KNO_3) were employed as the PCMs. Graphene oxide synthesized with several chemical processes were doped into salt solvent with two-step method firstly, and metal foam was impregnated with graphene seeded salt finally. The morphologies of the materials were analyzed by Scanning Electron Microscope (SEM), Fourier Transform Infrared Spectrometer (FTIR) and X-ray diffraction (XRD), and the thermal conductivities of the composite PCMs were theoretically predicted based on the correlations and models of the porous media. The thermal behaviors of all the materials were analyzed with DSC (differential scanning calorimeter), and the thermal stabilities and thermal effusivities were studied subsequently. It is highly indispensable to study the thermo-physical properties of the composite PCMs, which largely determine the performance and applicability of the LHTES system. And the LHTES system can be integrated into solar energy and geothermal energy utilization systems.

2. PREPARATION AND THERMAL CHARACTERIZATION

2.1. Graphene oxide and composite PCMs

The graphene oxide was produced from graphite powder involving several chemical processes by adopting the modified Hummer's method [26-27], which was done in controlled environment. Graphite powder (<20 μm, Sigma Aldrich, UK) was considered as the starting material. Sulphuric acid (H_2SO_4, concentration: 95%, VWR Chemicals, UK) and nitric acid (HNO_3, concentration: 69%, VWR Chemicals, UK) were used to oxidize graphite powder in water solution. As a typical synthesis procedure shown in **Figure 1 (a)**, 12 g of graphite powder was mixed with 100 mL H_2SO_4 and 50 mL HNO_3 in a conical flask, and the solution was kept on stirring for 24 h at a hot

plate of about 50 ºC. The reactants were synthesized with the addition of 100 mL of Deionized (DI) water, which were continuously magnetic stirring in a whole day. Then 12 g of potassium permanganate ($KMnO_4$, concentration: 99%, Sigma-Aldrich, UK) was slowly added to the above solution, and stirred in an ice bath of 0 ºC for 5 h. 60 mL of hydrogen peroxide (H_2O_2, concentration: 36%, Sigma-Aldrich, UK) was added, and the suspension was stirred overnight, which was conducted in the ice bath to keep the temperature low. Subsequently a filter paper (Whatman #42) was used to filter the resultant suspension. Then the filtrate from the solution was successively washed three times with hydrochloric acid (HCl, concentration: 10%, Sigma-Aldrich, UK) and DI water, which was then centrifuged with Heraeus Megafuge 16R (ThermoFisher Scientific, UK) at 13000 rpm for 1 h. After discarding the supernatant, the remaining material was then vacuum-dried overnight at 40 °C. Finally the graphene oxide nano-sheets were obtained.

$NaNO_3$ (Honeywell Fluka, UK), KNO_3 (Acros Organics, UK) and $NaNO_2$ (Honeywell Fluka, UK) were used as the base PCM, and the previous graphene and metal foam (Suzhou Longde Metal Foam Electronics Co. Ltd., CN; Porosity: 95.0%; Pore size: 10 pores per inch) were applied to enhance the thermo-physical properties of pure salt. **Table 1** lists the thermo-physical properties of HITEC salt, solar salt, graphene (subscript *np*), and metal foam [28-30]. **Figure 1 (b)** shows the synthesis process of the salt/graphene/metal foam composites, which was similar to that of the salt/Al_2O_3 nanopowder/metal foam composites in a previous research [31]. Firstly, $NaNO_2$, $NaNO_3$ and KNO_3 with mass ratios of 40:7:53 named HITEC salt was prepared and dissolved into DI water. Graphene with different mass fractions (1%, 2% or 3%) was suspended in the solution, respectively, which was then sonicated for 1 h (FB15057 ultrasonicator), so as to make good dispersion. Then the immersion of metal foam in a metal disc filled with the solution was carried out, which was sonicated with 10 mins to evacuate the air. The metal disc with the solution was

heated inside an eurotherm oven manufactured by Carbolite Sheffield at 200 ºC for 30 mins, then the salt/graphene/metal foam composite PCMs were obtained after naturally cooled. A similar method was used to synthesize the solar salt/graphene/metal foam composites, while $NaNO_3$ and KNO_3 with a mass ratio of 60:40 and a heating temperature of 250 °C were used instead. Series morphological and thermal characterization of the composites were addressed subsequently.

2.2. Morphological analysis

TEM (Transmission electron microscopy, FEI Tecnai TF20, Oxford Instruments, UK) was used to reveal the size of the synthesized graphene, so as to check whether the nanoparticles prepared are in nanoscale or not. Tabletop Microscope TM3030Plus (SEM, Hitachi High-Technology, Japan) was used to measure the surface characteristics of the composites on an uneven area, the modes of BSE and EDX were applied.

FTIR and XRD which investigates the functional groups presented in a specimen can analyze chemical bonding and molecular structure of the specimens. In the present study, Nicolet IS10 FT-IR spectrometer (ThermoFisher Scientific, UK) with a resolution of 4 cm^{-1} covers wavelength range of 400~4000 cm^{-1}, and gives the spectra of all the specimens at room temperature. The lab-based XRD used was a D8 powder diffractometer (Bruker, UK) with a Vantec detector (Cu-Ka source, 1.540 Å). The reflections of X-Rays was conducted by crystallographic atomic planes, and the operational voltage and applied current for the instrument were maintained at 40 kV and 40 mA, respectively. The specimen of about 0.5 g was prepared and filled in a shallow and circular holder, which was with the diameter of 4 cm and the depth of 1.5 cm. During the experiments, the total scanning time was 45 mins considering a step size of 0.035 º and a scanning range of 10-60 º, then the data were analyzed using X'Pert HighScore Plus software.

2.3. Techniques of thermal characterization

2.3.1. Characterization of effective thermal conductivity

Graphene used in the present study are with the density and thermal conductivity of 2200 kg m^{-3} and 5000 W $m^{-1}K^{-1}$, respectively [22], and the densities of the nanocomposites are shown in Supporting Information (**Table S1**). Nanoparticles can affect the thermal conductivity of the nanocomposite, which can be estimated with the theoretical models. The effective thermal conductivity of the nanocomposite (λ_{nc}) was calculated with the modified Maxwell-Garnett model [32-33], which considered the Brownian motion and nanoparticles aggregation and shown as follows:

$$\frac{\lambda_{nc}}{\lambda_{PCM}} = \frac{\lambda_{np} + 2\lambda_{PCM} - 2\Phi\left(\lambda_{PCM} - \lambda_{np}\right)}{\lambda_{np} + 2\lambda_{PCM} + \Phi\left(\lambda_{PCM} - \lambda_{np}\right)} + \frac{\rho_{np}\Phi c_{p\text{-}np}}{2\lambda_{PCM}}\sqrt{\frac{2K_B T_{nc}}{3\pi d_{np}\mu_{PCM}}} \quad (1)$$

where K_B is Boltzmann constant, d_{np} is nanoparticle size, which is 350 nm in the present study [34]. T_{nc} is the temperature of nanocomposite, and μ_{PCM} is the viscosity of pure salt. Based on the comparisons between the experimental measurements with steady state method and the theoretical predictions with models in the previous research [8], it has been proven that the models can accurately predict the thermal conductivities of the composite PCMs fabricated by metal foam. Thus the thermal conductivities of the salt/graphene/metal foam composites were theoretically predicted in the present study, due to the lack of steady state test device. A series of structural models were chosen based on the previous comparisons [35-37], as listed in **Table S2**.

2.3.2. Characterization of thermal behavior

The phase change behaviours of pure salt and composite PCMs were conducted with a Mettler-Toledo DSC (DSC1, Mettler Toledo Ltd., Leicester, UK), with the accuracy of temperature

measurement of ±0.02 ºC. The specimen was weighted using an Ultra-microbalance Mettler-Toledo balance (UMX2, Mettler Toledo, Leicester, UK) with an uncertainty of ±0.001 mg, and half of the crucible was filled to avoid the overflow issue. A standard aluminum crucible with 100 μL as the sample crucible was encapsulated with about 20.0~30.0 mg specimen, then the sample crucible and an empty crucible considered as the reference were symmetrically put into a platinum-iridium furnace. The heating method for HITEC salt and its composites was maintained at 50 ºC for 10 mins, ramped from 50 ºC to 200 ºC at a rate of 5 ºC min^{-1}, then kept isothermally for 10 mins at 200 ºC. While the cooling method was similar and ramped from 200 ºC to 50 ºC at a rate of -5 ºC min^{-1}, and the phase change of the specimens were characterized by both the extrapolated onset and peak temperatures. The thermal cycle for solar salt and its composites was similar, while the only difference was the temperature ranged from 100 ºC to 300 ºC.

The present DSC was also used to measure the specific heat of pure salt and its composites both in solid phase and liquid phase. The method followed to calculate the specific heat was the three-step procedure [38]. Firstly, the baseline heat flux (q_0) was recorded from two empty crucibles. Secondly, the heat flux (q_{sapphire}) was recorded from one crucible sealed with the standard sapphire and one empty one. Thirdly, the heat flux of the specimen was recorded (q_s), where one crucible sealed with the specimen was used instead of the sapphire crucible. The specific heat of the specimen ($c_{p,\,s}$) can be calculated as follows:

$$c_{p,\mathrm{s}} = c_{p,\,\text{sapphire}} \frac{\Delta q_{\mathrm{s}} / m_{\mathrm{s}}}{\Delta q_{\text{sapphire}} / m_{\text{sapphire}}} \tag{2}$$

In the present study, the salt and its composites were subjected to the same thermal procedure, that is, heated from 100 ºC to 300 ºC at 25.0 ºC min^{-1} and isothermal at 100 ºC and 300 ºC for 10 mins, respectively.

2.3.3. Thermo-gravimetric analysis and thermal effusivity

The weight of a specimen will be positively or negatively affected by the physical or chemical changes. Mettler-Toledo TGA (DSC1, Mettler Toledo Ltd., Leicester, UK) was used to detect the variation of mass correlated to temperature, and the operating temperature ranged from 40 °C to 850 °C at 10 °C min^{-1} in the present study. The ceramic crucibles were selected to adapt the materials and temperatures of the experiments, and about 5.00 to 10.00 mg specimens were loaded into the crucibles. Nitrogen purge gas with the purity of 99.99% was worked as carrier under a flow rate of 50 mL min^{-1}, which was controlled by a gas controller GC100.

The thermal effusivity of a material illustrates the capability of a material to exchange thermal energy with its surroundings [30, 38]. The thermal effusivity (e) is defined in Eq. (3).

$$e = \sqrt{\rho c_p \lambda} \tag{3}$$

The thermal effusivity consists of the heat capacity and heat transfer rate of the material, and is a critical physical quantity and a controlling parameter in describing the heat transfer performance in a number of industrial applications. In the present study, the thermal effusivities in both solid and liquid states were calculated respectively. For the calculation of thermal conductivity, 25 °C was considered in Eq. (1) in solid state, while 200 °C for HITEC salt and 250 °C for solar salt were considered in liquid state.

3. RESULTS AND DISCUSSION

3.1. Morphologies of composite PCMs

Figure 2 shows the morphologies of the graphene and composite PCMs characterized by TEM and SEM. The graphene shown in **Figure 2 (a)** is with the size of hundred nanometers, consists of

porous-like flakes. The SEM pictures of the salt/graphene nanocomposites are shown in **Figure 2 (b)**. It can be found that the sample shows a smooth appearance in large scale, and a granular appearance partially in the SEM pictures. As a result, distinguishing the nanoparticle (graphene) from salt becomes difficult. **Figure 2 (c)** and **(d)** shows the samples of the salt/graphene/metal foam composites. It can be seen that there is no separation between the nanocomposite and metal foam, and the existence of the elements Cu, Na, K, N has been verified in the EDS spectrum. In addition, a dimensionless parameter α [39] is employed to evaluate the compatibility between the nanocomposite and metal foam, where the parameter reflects the ratio of the actual mass to the ideal one of the nanocomposite impregnated into the porous metal foam. It was found that the impregnation ratio can reach above 90.0% in the present study.

Figure 3 (a) shows FT-IR absorption spectra of pure salts, the salt/graphene nanocomposites and salt/graphene/metal foam composites. The peaks in FTIR spectra (**Figure 3 (a-I)**) for HITEC salt and its composite PCMs are observed at 835 cm^{-1}, 1228 cm^{-1}, 1370 cm^{-1}, 1763 cm^{-1} and 2396 cm^{-1}, while the peaks in FTIR spectra (**Figure 3 (a-II)**) for solar salt and its composite PCMs are observed at 834 cm^{-1}, 1345 cm^{-1}, 1763 cm^{-1}, 1789 cm^{-1} and 2428 cm^{-1}. The difference should be attributed to the element of sodium nitrite ($NaNO_2$) in HITEC salt. It can be seen that no apparent difference of FT-IR absorption spectra are found for all the specimens fabricated by the same salt, indicating that the physical bonding of graphene with nitrate or nitrite exist does not interrupt the chemical structure interaction. Thus graphene can mix well with salt, similarly to other nanoparticles [40]. In addition, FT-IR absorption spectra also indicate that the salt/graphene/metal foam composite has no occurrence of new structure.

Figure 3 (b) presents XRD patterns of pure salts, the salt/graphene nanocomposites and salt/graphene/metal foam composites. It can be seen from the pattern of HITEC salt that,

characteristic peaks appear at 19.35°, 23.86°, 29.72°, 32.30°, 34.11°, 41.45°, 44.77° and 51.41°. While characteristic peaks appear at 23.94°, 29.52°, 32.14°, 39.19° and 48.13° from the pattern of solar salt. The appearance and disappearance of peaks correspond to the relevant elements. Other characteristic diffraction peaks of the composite PCMs are nearly the same as those of pure salt. It can be concluded that the salt remains intact in the metal foam without chemical reaction, and is also not greatly affected by graphene. As a result, all combinations are formed by physical action. However, it can be seen from **Figure 3 (b)** that new peaks marked in rectangular regions appear at around 26~28° in the patterns of the salt/graphene/metal foam composites. Those peaks should be an indication of the appearance of nickel or copper element.

3.2. Thermal characterization of composite PCMs

3.2.1. Effective thermal conductivities of composite PCMs

Figure 4 shows the calculations of the effective thermal conductivities of the composite PCMs, which were considered in solid state (T=25 °C). It is shown that the effective thermal conductivities of the salt/graphene nanocomposites increase slightly. The effective thermal conductivities of HITEC salt/graphene nanocomposites are 1.045 W $m^{-1}K^{-1}$, 1.091 W $m^{-1}K^{-1}$ and 1.137 W $m^{-1}K^{-1}$ with the addition of 1 wt.%, 2 wt.% and 3 wt.% graphene, respectively, while those of solar salt/graphene nanocomposites are 1.049 W $m^{-1}K^{-1}$, 1.099 W $m^{-1}K^{-1}$ and 1.150 W $m^{-1}K^{-1}$. The phenomenon is a little higher than those in the literature [40-41], e.g., the thermal conductivity of solar salt/1 wt.% Fe_2O_3 nanocomposite is 0.828 W $m^{-1}K^{-1}$ [40], while the thermal conductivity of solar salt/0.5 wt.% MgO nanocomposite is 0.853 W $m^{-1}K^{-1}$ [41]. The reason is that the thermal conductivities of the iron oxide and magesium oxide are slightly lower than that of graphene. Similarly, the addition of 1~3 wt.% graphene slightly increases the effective thermal conductivities

of the salt/metal foam composites, i.e., the effective thermal conductivities of the salt/nickel foam composites and salt/copper foam composites can be enhanced by 8~16% and 26~49%, respectively. Moreover, the effective thermal conductivities of the salt/graphene/metal foam composites are greatly enhanced, e.g., the effective thermal conductivity of HITEC salt/3 wt.% graphene/copper foam composite can reach approximate 8.7 W $m^{-1}K^{-1}$, indicating about 1140% increment in comparison with HITEC salt; While that of HITEC salt/3 wt.% graphene/nickel foam composite can reach approximate 3.0 W $m^{-1}K^{-1}$, indicating about 330% increment in comparison with HITEC salt. Therefore, there are apparent difference between the effective thermal conductivities of the salt/graphene/copper foam composites and those of the salt/graphene/nickel foam composites, which is caused by the higher thermal conductivity of copper skeleton, as listed in **Table 1**. However, because of corrosion issue of copper induced by salt, the balance related to the thermal conductivity and thermal stability should be considered in practical application. It can be concluded that the composite PCMs with good thermal characteristics can be the effective media in the application of LHTES system, given that metal foam provides conductive paths for heat transfer. In addition, in a preliminary pilot test, it is found that the time-duration of solar salt/2 wt.% graphene/copper foam composite for heat storage is considerably reduced by about 75.0%, in comparison with that of pure solar salt, which verifies the large thermal conductivity of the composite PCMs.

3.2.2. Phase change behaviors of composite PCMs

The phase change temperatures and latent heats of pure salts, the salt/graphene nanocomposites and salt/graphene/metal foam composites were obtained with DSC. **Figure 5** shows the values of the phase change temperatures of pure salts and composite PCMs. With the addition of graphene, the extrapolated onset melting temperatures and onset freezing temperatures of pure salts can be

slightly decreased and increased, respectively, e.g., for HITEC salt/3 wt.% graphene nanocomposite, the extrapolated onset melting temperature and onset freezing temperature shift from 138.67 ºC and 141.79 ºC to 137.27 ºC and 142.08 ºC, respectively, in comparison with those of HITEC salt; While for solar salt/3 wt.% graphene nanocomposite, the extrapolated onset melting temperature and onset freezing temperature shift from 220.82 ºC and 227.29 ºC to 219.31 ºC and 227.45 ºC, respectively, in comparison with those of solar salt. The early occurrence of phase change is mainly because of the good combination and dispersion performance of the salt and nanoparticles [38], as depicted in **Figure 2 (b)**. The combined effects of metal foam and graphene induce the variations of phase change temperatures of the salt/graphene/metal foam composites to some extent. It can be seen that for HITEC salt, the melting/freezing phase change temperatures of the salt/graphene/copper foam composites deviate from 1.11 ºC maximumly, whereas that of the salt/graphene/nickel foam composites is about 0.69 ºC. For solar salt, the melting/freezing phase change temperatures of the salt/graphene/copper foam composites deviate from 4.13 ºC maximumly, whereas that of the salt/graphene/nickel foam composites is about 4.96 ºC.

Figure 6 shows the variations of latent heats for pure salts and the composite PCMs. Three measurements were done to ensure the repeatability and accuracy of the results. The latent heats of the salt/metal foam composites decrease significantly as metal skeleton does not undergo the phase change process, e.g., the latent heat of HITEC salt/nickel foam composite decreases from 60.62 kJ kg^{-1} to 48.37 kJ kg^{-1}, while that of solar salt/nickel foam composite decreases from 108.39 kJ kg^{-1} to 77.47 kJ kg^{-1}, in comparison with that of pure salt. The addition of graphene can slightly affect the latent heats of the salt and salt/metal foam composites, e.g., the latent heats of HITEC salt and HITEC salt/nickel foam composite decrease to 57.59 kJ kg^{-1} and 46.32 kJ kg^{-1} with the addition of 3 wt.% graphene, respectively; while those of solar salt and solar salt/nickel foam

composite decrease to 104.59 kJ kg^{-1} and 74.53 kJ kg^{-1} with the addition of 3 wt.% graphene, respectively. The phenomenon of the slight decrease of latent heat can be attributed to the two reasons. On one hand, the mass fraction of graphene is very small and within 3%, which should reduce the latent heat slightly. On the other hand, the increase of the interfacial thermal resistance caused by the interface between the salt and graphene might affect the latent heat to some extent [42]. A compromise between the metal foam and graphene should be considered to get the suitable thermo-physical properties of the composite PCMs in practical application.

3.2.3. Specific heats of composite PCMs

Table 2 lists the mean specific heats of HITEC salt, the salt/graphene nanocomposites and salt/graphene/metal foam composites. The specific heats in solid and liquid states were calculated within the temperature range of 105~110 ºC and 180~290 ºC, respectively. It can be seen that with the addition of graphene, the specific heats of the nanocomposites are enhanced both in solid and liquid states, e.g., the specific heats of HITEC salt/3 wt.% graphene nanocomposite are 1.463 kJ $kg^{-1}K^{-1}$ and 1.601 kJ $kg^{-1}K^{-1}$ in solid and liquid states, compared to those of HITEC salt of 1.415 kJ $kg^{-1}K^{-1}$ and 1.562 kJ $kg^{-1}K^{-1}$, respectively. It can be summaried that the enhancements are about 0.80~3.39% in solid state, and -1.43~2.47% in liquid state with the graphene concentration of 1~3 wt.%. Furthermore, the specific heat enhancements are compared with those in the literature [43], as listed in **Table S3**. The enhancements are a little lower than those in the relevant work, which is mainly due to the type, size and concentration of the nanoparticles. In contrast, the specific heats of the salt/graphene/metal foam composites decrease, in comparison with that of HITEC salt, which is due to the inclusion of metal foam. It is found that the weaknesses of specific heat are about 0~12.01% in solid state, and 0.80~11.61% in liquid state totally.

Table 3 lists the mean specific heats of solar salt, the salt/graphene nanocomposites and salt/graphene/metal foam composites. The specific heats in solid and liquid states were calculated within the temperature range of 150~200 ºC and 260~290 ºC, respectively. It can be seen that with the addition of graphene, the specific heats of the nanocomposites are also slightly enhanced in solid state, e.g., the specific heat of solar salt/3 wt.% graphene composite is 1.843 kJ $kg^{-1}K^{-1}$ in solid state, compared to that of solar salt of 1.830 kJ $kg^{-1}K^{-1}$. It can be seen that the enhancements are about 0.05~2.45% in solid state with graphene concentration of 1~3 wt.%, which are lower to be -7.46~-0.27% in liquid state. Similarly, **Table S3** lists the comparisons of specific heat enhancements with those in the literature [13, 40, 41, 44-47]. As different types, sizes and concentrations of the nanoparticles were used by the researchers, diverse enhancements are presented accordingly. The specific heat enhancements in the present study show general agreement with the relevant works. Additionally, the same tendency is found between current study and the study of Awad et al. [40], that is, the specific heat enhancements become lower in liquid state than those in solid state. On the contrary, the specific heats of the salt/graphene/metal foam composites decrease similarly, compared to that of solar salt, due to the inclusion of metal foam. It is found that the weaknesses of specific heat are about 3.81~19.48% in solid state, and 5.56~18.81% in liquid state.

The phenomenon of the increase of specific heats for the salt/graphene nanocomposites can be attributed to the following reasons. Graphene nanoparticles strongly interact with the molten salt molecules around, and contribute to form the nanostructure named compressed layer with extremely large specific surface area [13, 42, 48-49]. This different structural characteristics cause large intermolecular force together with the increased surface energy, and induce the enhancement of the effective specific heat subsequently. Additionally, the interfacial thermal

resistance of the nanostructure between the salt and graphene will increase with the increased surface area to some extent [42], but it will not affect the total thermal resistance of the composite PCMs. Further molecular dynamics simulation and heat transfer analysis are needed to clarify the mechanism of the enhancement of specific heat.

3.2.4. Thermo-gravimetric analyses of composite PCMs

Figure 7 shows the thermo-gravimetric analyses of pure salts and salt/graphene/metal foam composites. It can be seen that the tendency of two type of salts and their composites are similar. There is no mass descending until 300 °C, indicating that the samples are totally dry for the experiments. HITEC salt is stable up to about 540 °C, then rapid degradation of the salt appears, as shown in **Figure 7 (a)**. It can be seen that nearly 60% of the mass loses between 550°C and 800°C. The mass remain percentage at 800 °C for HITEC salt, HITEC salt/1 wt.% graphene, HITEC salt/2 wt.% graphene and HITEC salt/3 wt.% graphene are 41.39%, 44.40%, 48.19% and 53.27%, respectively. The larger percentages of HITEC salt/graphene composites might be due to the inclusion of graphene, which can exist over 800 °C. A solid stable compound may be produced as the mass slightly changes above 800°C, e.g., the mass remain percentage of HITEC salt at 850 °C is 39.74%. Because all the TGA tests were conducted under the atmosphere of nitrogen to avoid oxidation, and most of the mass loss happens through the release of nitrogen and oxygen gases. The remain mass in the crucible might be a mixture of sodium and potassium oxide. Furthermore, the salt/graphene/metal foam composites show larger mass left at the final stage, as the metal skeleton (nickel or copper) can be kept over 850 °C [50-51].

It can be seen from **Figure 7 (b)** that solar salt is also stable up to about 590 °C, then rapid degradation appears. Similarly, the salt/graphene nanocomposites are with larger percentages of

mass at 800 ºC, in comparison with that of pure solar salt. The salt/graphene/metal foam composites show larger mass left finally because of the metal skeleton (nickel or copper), almost 65.0% and 75.0% for the salt/3 wt.% graphene/nickel foam composite and the salt/3 wt.% graphene/copper foam composites. However, it can be seen from **Figure 7** that the mass remain percentages of the salt/graphene composites below 600 ºC are slightly lower than that of pure salt, which might be caused by the tolerance of the experiments.

3.2.5. Thermal stabilities of composite PCMs

The stabilities of the salt/3 wt.% graphene/metal foam composites were determined with DSC, which were performed similarly to section 3.2.2 of thermal behaviour characterization. **Figure S1** shows examples of the curves of fifty thermal cycles, and it can be seen that the peaks belongs to solid-solid phase change are obvious in several thermal curves at the beginning, but those peaks degrade in the following thermal cycles. However, the solid-liquid phase change can be kept well with the thermal cycles, and slight changes are found after the circulations. It is found that the phase change temperatures together with latent heats of the composite PCMs after fifty thermal cycles are almost the same as those shown in **Figures 5** and **6**, indicating that the samples are with good stabilities. Furthermore, the morphologies of the sample before and after thermal cycles indicates that slightly separation between graphene and salt appears after fifty cycles. A preliminary pilot test shows that the temperature evolutions appear almost no difference after several heat storage/retrieval processes.

3.3. Thermal effusivities of composite PCMs

The effusivities of pure salts, the salt/graphene nanocomposites and salt/graphene/metal foam composites are calculated, and the results both in solid and liquid states are listed in **Tables 2** and

3. Here, only the thermal conductivities calculated with the model of Calmidi and Mahajan were considered [35]. Generally, because of the good thermo-physical properties of graphene, the present effusivities of the nanocomposites are slightly larger than those in the literature, e.g., the effusivities of the solar salt/1 wt.% Fe_2O_3 nanocomposite are 1.636 kJ $m^{-2}K^{-1}s^{-1/2}$ and 1.301 kJ $m^{-2}K^{-1}s^{-1/2}$ in solid and liquid states [40], in comparison with those of the solar salt/1 wt.% graphene nanocomposite of 2.023 kJ $m^{-2}K^{-1}s^{-1/2}$ and 1.794 kJ $m^{-2}K^{-1}s^{-1/2}$, respectively. It can be seen that the effusivities of the composite PCMs are larger than those of pure salt, e.g., the effusivities of HITEC salt/3 wt.% graphene/copper foam composite are 5.11 kJ $m^{-2}K^{-1}s^{-1/2}$ in solid state and 5.27 kJ $m^{-2}K^{-1}s^{-1/2}$ in liquid state, while those of HITEC salt are 1.43 kJ $m^{-2}K^{-}s^{-1/2}$ and 1.15 kJ $m^{-2}K^{-1}s^{-1/2}$ in solid and liquid states, respectively. It is due to the reason that although the specific heats of the salt/graphene nanocomposites and salt/metal foam composites decrease slightly, the thermal conductivities of those composite PCMs increase. It can be concluded that the effusivities of the salt/graphene/metal foam composites can be increased by 110~270% in solid state and 150~360% in liquid state, respectively. Furthermore, as the inclusion of metal foam greatly increases the thermal conductivities of pure salts (shown in **Figure 4**), the thermal effusivities of the salt/graphene/metal foam composites are larger than those of the salt/graphene nanocomposites, which benefits heat storage. The potential application of the salt/graphene/metal foam composites can increase the heat storage/retrieval rates of the LHTES system, inducing the high power and energy efficiency of the system.

It can be seen from **Table 2** that the thermal effusivities of HITEC salt and its composite PCMs are almost the same in solid and liquid states, which is because that the density and thermal conductivity of HITEC salt are larger in solid state than those in liquid state, but the specific heat of HITEC salt is lower in solid state than that in liquid state. However, **Table 3** show that the

thermal effusivities of solar salt and its composite PCMs are very different between solid and liquid states, which is because that the density, thermal conductivity and specific heat of solar salt are larger in solid state than those in liquid state. Therefore, the characteristics of different thermal effusivities in solid and liquid states should be considered in the selection of PCMs used in the real temperature range. Moreover, the addition of graphene and metal foam can restrict the flow of liquid salt, and retrieve the issue of the leakage accordingly, which provides a new strategy for obtaining shape-stabilized PCMs applied for thermal energy storage.

4. CONCLUSIONS

In the present study, HITEC salt and solar salt were used as the pure PCMs, and graphene and metal foam were combined to enhance pure salts. The composite PCMs were synethesized and morphologically and thermally characterized, and the conclusions can be drawn as follows:

(1) The salt/graphene nanocomposite is totally compatible with metal foam, and no obvious changes of wavelength peaks are found with FT-IR analyses. Small peaks appear in XRD pattern of the salt/graphene/metal foam composites due to the addition of metal elements.

(2) The effective thermal conductivities of the salt/graphene/metal foam composites are greatly enhanced, while those of the salt/graphene nanocomposites are slightly enhanced, in comparison with that of pure salt. A preliminary pilot test indicates that the time-duration of solar salt/2 wt.% graphene/copper foam composite for heat storage can be considerably reduced by about 75.0%, in comparison with that of pure solar salt.

(3) With the addition of graphene, the extrapolated onset melting temperatures and onset freezing temperatures of pure salts can be slightly decreased and increased, respectively. The maximum deviation of the melting/freezing phase change temperatures of the HITEC

salt/graphene/copper foam composites is 1.11 °C, whereas that of the solar salt/graphene/copper foam composites is 4.13 °C. The specific heats of the salt/graphene nanocomposites are enhanced with the addition of graphene in solid state.

(4) Thermo-gravimetric analyses indicate that HITEC salt and solar salt are stable up to about 540 °C and 595 °C, respectively. Slight changes of phase change temperature and latent heat are found after the composite PCMs underwent fifty melting-freezing cycles, indicating the good stabilities of the composites. The effusivities of the salt/graphene/metal foam composites are larger than those of pure salt, indicating the increments of 110~270% in solid state and 150~360% in liquid state, respectively.

Consequently, the investigations of thermo-physical properties of the nanocomposites with porous media will lead to guide the design and model of the thermal energy storage system and improve the performance of the system accordingly. In other words, it will extend the application of nanoparticles in thermal energy storage.

ASSOCIATED CONTENT

Supporting Information

The following files:

Densities and volume fractions of the salt/graphene nanocomposites; Correlations and models of effective thermal conductivities of the composite PCMs; Comparisons of specific heats with the results in the literature; Repeated DSC curves of the salt/graphene/metal foam composites (PDF)

AUTHOR INFORMATION

Corresponding Authors

*E-mail: xiaoxin2010@alumni.sjtu.edu.cn

**E-mail: d.wen@buaa.edu.cn

ORCID

Xin Xiao: 0000-0003-0718-2591

Hongwei Jia: 0000-0001-7726-1370

Shahid Pervaiz: 0000-0002-6861-9374

Dongsheng Wen: 0000-0003-3492-7982

Notes

The authors declare no competing financial interest.

ACKNOWLEDGMENT

The authors would like to acknowledge the support of EU Marie Sklodowska-Curie International Incoming Fellowship (Project reference: 706788) and the European Research Council Consolidator Grant (ERC2014-CoG, Project reference: 648375).

REFERENCES

[1] Pelay, U.; Luo, L.; Fan, Y. L.; Stitou, D.; Rood, M. Thermal energy storage systems for concentrated solar power plants. *Renew. Sustain. Energy Rev.* **2017**, 79, 82–100.

[2] Kuravi, S.; Trahan, J.; Goswami, D. Y.; Rahman, M. M.; Stefanakos, E K. Thermal energy storage technologies and systems for concentrating solar power plants. *Prog. Energy Combust. Sci.* **2013**, 39, 285–319.

[3] Zhang, P.; Xiao, X.; Ma, Z. W. A review of the composite phase change materials: Fabrication, characterization, mathematical modeling and application to performance enhancement. *Appl. Energy* **2016**, 165, 472–510.

[4] Zhu, S. L.; Nguyen, M. T.; Tokunaga, T.; Yonezawa, T. Size-tunable alumina-encapsulated Sn-based phase change materials for thermal energy storage. *ACS Appl. Nano Mater.* **2019**, 2, 3752−3760.

[5] Liu, M. L.; Ma, Y. Y.; Wu, H. W.; Robert Y. Wang, R. Y. Metal matrix-metal nanoparticle composites with tunable melting temperature and high thermal conductivity for phase-change thermal storage. *ACS Nano* **2015**, 9, 1341-1351.

[6] Kholmanov, I.; Kim, J. Y.; Ou, E.; Ruoff, R. S.; Shi, L. Continuous carbon nanotube-ultrathin graphite hybrid foams for increased thermal conductivity and suppressed subcooling in composite phase change materials. *ACS Nano* **2015**, 9, 11699–11707.

[7] Wang, C. M.; Wang, T. J.; Hu, Z. J.; Cai, Z. Y. Facile synthesis and thermal performance of cety palmitate/nickel foam composite phase change materials for thermal energy storage. *J. Energy Storage* **2020**, 28, 101179.

[8] Xiao, X.; Zhang, P.; Li, M. Effective thermal conductivity of open-cell metal foams impregnated with pure paraffin for latent heat storage. *Int. J. Therm. Sci.* **2014**, 81, 94–105.

[9] Feng, S. S.; Zhang, Y.; Shi, M.; Wen, T.; Lu, T. J. Unidirectional freezing of phase change materials saturated in open-cell metal foams. *Appl. Therm. Eng.* **2015**, 88, 315–321.

[10] Riazi, H.; Murphy, T.; Webber, G. B.; Atkin, R.; Tehrani, S. S. M.; Taylor, R. A. Specific heat control of nanofluids: a critical review. *Int. J. Therm. Sci.* **2016**, 107, 25–38.

[11] Tran, N.; Zhao, W. Y.; Carlson, F.; Davidson, J. H.; Stein, A. Metal nanoparticle−carbon matrix composites with tunable melting temperature as phase-change materials for thermal energy storage. *ACS Appl. Nano Mater.* **2018**, 1, 1894−1903.

[12] Tiznobaik, H.; Banerjee, D.; Shin, D. Effect of formation of "long range" secondary dendritic nanostructures in molten salt nanofluids on the values of specific heat capacity. *Int. J. Heat Mass Transf.* **2015**, 91, 342–346.

[13] Riazi, H.; Mesgari, S.; Ahmed, N. A.; Taylor, R. A. The effect of nanoparticle morphology on the specific heat of nanosalts. *Int. J. Heat Mass Transf.* **2016**, 94, 254–261.

[14] Song, W. L.; Lu, Y. W.; Wu, Y. T.; Ma, C. F. Effect of SiO_2 nanoparticles on specific heat capacity of low-melting-point eutectic quaternary nitrate salt. *Sol. Energy Mater. Sol. Cells* **2018**, 179, 66–71.

[15] Zhang, H. F.; Shin, D. Y.; Santhanagopalan, S. Microencapsulated binary carbonate salt mixture in silica shell with enhanced effective heat capacity for high temperature latent heat storage. *Renew. Energy* **2019**, 134, 1156–1162.

[16] Choi, H. J.; Jung, S. M.; Seo J. M.; Chang, D. W.; Dai, L. M.; Baek, J. B. Graphene for energy conversion and storage in fuel cells and supercapacitors. *Nano Energy* **2012**, 1, 534–551.

[17] Pop, E.; Varshney, V.; Roy, A. K. Thermal properties of graphene: Fundamentals and applications. *MRS Bull*. **2012**, 37, 1273.

[18] Allahbakhsh, A.; Arjmand, M. Graphene-based phase change composites for energy harvesting and storage: State of the art and future prospects. *Carbon* **2019**, 148, 441–480.

[19] Liu, Y. J.; Zhang, D. Effect of covalent functionalization and phase change matrix on heat transfer across graphene/phase change material interfaces. *Appl. Therm. Eng.* **2019**, 151, 38–45.

[20] Yang, J.; Qi, G. Q.; Liu, Y.; Bao, R. Y.; Liu, Z. Y.; Yang, W.; Xie, B. H.; Yang, M. B. Hybrid graphene aerogels/phase change material composites: Thermal conductivity, shape-stabilization and light-to-thermal energy storage. *Carbon* **2016**, 100, 693–702.

[21] Chen, D. Z.; Qin, S. Y.; Tsui, G. C. P.; Tang, C. Y.; Ouyang, X.; Liu, J. H.; Tang, J. N.; Zuo, J. D. Fabrication, morphology and thermal properties of octadecylamine-grafted graphene oxide-modified phase-change microcapsules for thermal energy storage. *Composites Part B* **2019**, 157, 239–247.

[22] Kant, K.; Shukla, A.; Sharma, A.; Biwole, P. H. Heat transfer study of phase change materials with graphene nanoparticle for thermal energy storage. *Sol. Energy* **2017**, 146, 453–463.

[23] Yuan, P.; Zhang, P.; Liang, T.; Zhai, S. P. Effects of surface functionalization on thermal and mechanical properties of graphene/polyethylene glycol composite phase change materials. *Appl. Surf. Sci.* **2019**, 485, 402–412.

[24] Ho, M. X.; Pan, C. Experimental investigation of heat transfer performance of molten HITEC salt flow with alumina nanoparticles. *Int. J. Heat Mass Transf.*. 2017, 107, 1094-1103.

[25] Loo, K.V.; Lapauw, T.; Ozalp, N.; Strom, E.; Lambrinou, K.; Vleugels, J. Compatibility of SiC--and MAX phase-based ceramics with a KNO_3-$NaNO_3$ molten solar salt. *Sol. Energy Mater. Sol. Cells* **2019**, 195, 228-240.

[26] Hummers, Jr. W. S.; Offeman, R. E. Preparation of graphitic oxide. *J Am. Chem. Soc.* **1958**, 80, 1339.

[27] Abdelkader, A. M.; Valles, C.; Cooper, A. J.; Kinloch, I. A.; Dryfe, R. A. W. Alkali reduction of graphene oxide in molten halide salts: production of corrugated graphene derivatives for high-performance supercapacitors. *ACS Nano* **2014**, 8, 11225–11233.

[28] Janz, G.; Krebs, U.; Siegenthaler, H.; Tomkins, R. Molten salts: volume 3 nitrates, nitrites, and mixtures: electrical conductance, density, viscosity, and surface tension data. *J. Phys. Chem. Ref. Data* **1972**, 1, 581–746.

[29] Zhang P, Xiao X, Meng Z N, Li M. Heat transfer characteristics of a molten-salt thermal energy storage unit with and without heat transfer enhancement. *Appl. Energy* **2015**, 137, 758–772.

[30] Yang, S. M.; Tao W. Q. Heat transfer. 3rd ed. Beijing: Higher Education Press; **2002**.

[31] Xiao, X.; Jia, H. W.; Wen, D. S.; Zhao, X. D. Thermal performance analysis of a solar energy storage unit encapsulated with HITEC salt/copper foam/nanoparticles composite. *Energy* **2020**, 192, 116593.

[32] Xuan, Y. M.; Li, Q.; Hu, W. F. Aggregation structure and thermal conductivity of nanofluids. *AIChE J.* **2003**, 49, 1039–1043.

[33] Jouybari, H. J.; Saedodin, S.; Zamzamian, A.; Nimvari, M. E.; Wongwises, S. Effects of porous material and nanoparticles on the thermal performance of a flat plate solar collector: An experimental study. *Renew. Energy* **2017,** 114, 1407–1418.

[34] Xiao, X.; Zhang, G.; Ding, Y. L.; Wen, D. S. Rheological characteristics of molten salt seeded with Al_2O_3 nanopowder and graphene. *Energies* **2019**, 12, 467.

[35] Calmidi, V. V.; Mahajan, R. L. The effective thermal conductivity of high porosity fibrous metal foams. *ASME J. Heat Transfer* **1999**, 121, 466–471.

[36] Dul'nev, G. N. Heat transfer through solid disperse systems. *J. Eng. Phys. Thermophys.* **1965**, 9, 399–404.

[37] Singh, R.; Kasana, H. S. Computational aspects of effective thermal conductivity of highly porous metal foams. *Appl. Therm. Eng.* **2004**, 24, 1841–1849.

[38] Xiao, X.; Zhang, P. Morphologies and thermal characterization of paraffin/carbon foam composite phase change material. *Sol. Energy Mater. Sol. Cells* **2013**, 117, 451–461.

[39] Xiao, X.; Zhang, P.; Li, M. Preparation and thermal characterization of paraffin/metal foam composite phase change material. *Appl. Energy* **2013**, 112, 1357–1366.

[40] Awad, A.; Navarro, H.; Ding, Y. L.; Wen, D. S. Thermal-physical properties of nanoparticle-seeded nitrate molten salts. *Renew. Energy* **2018**, 120, 275.

[41] Saranprabhu, M. K.; Rajan, K. S. Magnesium oxide nanoparticles dispersed solar salt with improved solid phase thermal conductivity and specific heat for latent heat thermal energy storage. *Renew. Energy* **2019**, 141, 451–459.

[42] Hu, Y. W.; He, Y. R.; Zhang, Z. D.; Wen, D. S. Effect of Al_2O_3 nanoparticle dispersion on the specific heat capacity of a eutectic binary nitrate salt for solar power applications. *Energy Convers. Manage.* **2017**, 142, 366–373.

[43] Ho, M. X.; Pan, C. Optimal concentration of alumina nanoparticles in molten Hitec salt to maximize its specific heat capacity. *Int. J. Heat Mass Transf.* **2014**, 70, 174–184.

[44] Dudda, B.; Shin, D. Effect of nanoparticle dispersion on specific heat capacity of a binary nitrate salt eutectic for concentrated solar power applications. *Int. J. Therm. Sci.* **2013**, 69, 37–42.

[45] Chieruzzi, M.; Cerritelli, G. F.; Miliozzi, A.; Kenny, J. M. Effect of nanoparticles on heat capacity of nanoflfluids based on molten salts as PCM for thermal energy storage. *Nanoscale Res. Lett.* **2013**, 8, 448.

[46] Lu, M. C.; Huang, C. H. Specific heat capacity of molten salt-based. *Nanoscale Res. Lett.* **2013**, 8, 292.

[47] Andreu-Cabedo, P.; Mondragon, R.; Hernandez, L.; Martinez-Cuenca, R.; Cabedo, L.; Julia, J. E. Increment of specific heat capacity of solar salt with SiO_2 nanoparticles. *Nanoscale Res. Lett.* **2014**, 9, 582.

[48] Seo, J. H.; Shin, D. H. Size effect of nanoparticle on specific heat in a ternary nitrate ($LiNO_3$–$NaNO_3$–KNO_3) salt eutectic for thermal energy storage. *Appl. Therm. Eng.* **2016**, 102, 144–148.

[49] Yuan, F.; Li, M. J.; Qiu, Y.; Ma, Z.; Li, M. J. Specific heat capacity improvement of molten salt for solar energy applications using charged single-walled carbon nanotubes. *Appl. Energy* **2019**, 250, 1481–1490.

[50] Lasfargues, M. Nitrate based high temperature nano-heat-transfer-fluids: formulation & characterisation. PhD dissertation. University of Leeds, **2014**.

[51] Stern, H. K. High temperature properties and decomposition of inorganic salts nitrates and nitrites. *J. Phys. Chem. Ref. Data* **1972**, 1, 747–772.

Table 1 Thermo-physical properties of pure salt, metal foam and graphene used in the present study

		HITEC salt [28]	Solar salt [28-29]	Graphene [22]		Metal foam		
							Nickel foam [30]	Copper foam [30]
Density ($kg\ m^{-3}$)	Solid	2065.5	2079.0	Density ($kg\ m^{-3}$)	2200	Porosity	95%	95%
	Liquid	1936.0	1884.0					
Melting point (°C)		140~142	218~228	Thermal conductivity ($W\ m^{-1}K^{-1}$)	5000	Pore size	10 PPI	10 PPI
Thermal conductivity ($W\ m^{-1}K^{-1}$)	Solid	0.70	0.705	Specific heat ($kJ\ kg^{-1}K^{-1}$)	0.79	Skeleton density ($kg\ m^{-3}$)	8900	8930
	Liquid	0.4366	0.478					
Dynamic viscosity ($kg\ m^{-1}s^{-1}$)		0.00787	0.00506			Skeleton thermal conductivity ($W\ m^{-1}K^{-1}$)	91.4	398

Table 2 Specific heats and thermal effusivities of pure HITEC salt, salt/graphene nanocomposites and salt/graphene/metal foam composites

	c_{ps} (kJ kg^{-1}K^{-1}) (105-110 °C)	c_{pl} (kJ kg^{-1}K^{-1}) (180-290 °C)	e_s (kJ m^{-2}K^{-1}s$^{-1/2}$)	e_l (kJ m^{-2}K^{-1}s$^{-1/2}$)
Pure HITEC salt	1.415	1.562	1.430	1.149
HITEC salt/1 wt.% graphene	1.440	1.540	1.763	1.777
HITEC salt/2 wt.% graphene	1.426	1.563	1.794	1.841
HITEC salt/3 wt.% graphene	1.463	1.601	1.855	1.913
HITEC salt/1 wt.% graphene/nickel foam	1.274	1.422	3.003	3.099
HITEC salt/2 wt.% graphene/nickel foam	1.422	1.554	3.202	3.275
HITEC salt/3 wt.% graphene/nickel foam	1.303	1.427	3.094	3.180
HITEC salt/1 wt.% graphene/copper foam	1.336	1.495	5.262	5.428
HITEC salt/2 wt.% graphene/copper foam	1.270	1.391	5.149	5.261
HITEC salt/3 wt.% graphene/copper foam	1.245	1.381	5.115	5.266

Table 3 Specific heats and thermal effusivities of pure solar salt, salt/graphene nanocomposites and salt/graphene/metal foam composites

	c_{ps} (kJ kg^{-1}K^{-1}) (150-200 °C)	c_{pl} (kJ kg^{-1}K^{-1}) (260-290 °C)	e_s (kJ m^{-2}K^{-1} s$^{-1/2}$)	e_l (kJ m^{-2}K^{-1} s$^{-1/2}$)
Pure solar salt	1.830	1.677	1.638	1.229
Solar salt/0.5 wt.% Fe_2O_3[a]	1.570	1.394	1.819	1.583
Solar salt/0.5 wt.% CuO[a]	1.530	1.377	1.693	1.425
Solar salt/1 wt.% graphene	1.875	1.605	2.023	1.794
Solar salt/1 wt.% Fe_2O_3[a]	1.560	1.400	1.636	1.301
Solar salt/1 wt.% CuO[a]	1.520	1.343	1.151	1.203
Solar salt/2 wt.% graphene	1.831	1.551	2.047	1.817
Solar salt/3 wt.% graphene	1.843	1.672	2.101	1.940
Solar salt/1 wt.% graphene/nickel foam	1.760	1.583	3.542	3.238
Solar salt/2 wt.% graphene/nickel foam	1.591	1.430	3.402	3.117
Solar salt/3 wt.% graphene/nickel foam	1.729	1.553	3.582	3.291
Solar salt/1 wt.% graphene/copper foam	1.474	1.371	5.543	5.145
Solar salt/2 wt.% graphene/copper foam	1.715	1.510	6.001	5.426
Solar salt/3 wt.% graphene/copper foam	1.515	1.361	5.663	5.177

[a] The results from Awad et al. [40] are also included for comparison, which clearly indicates that the thermal effusivities of the composite PCMs in the present study are improved significantly.

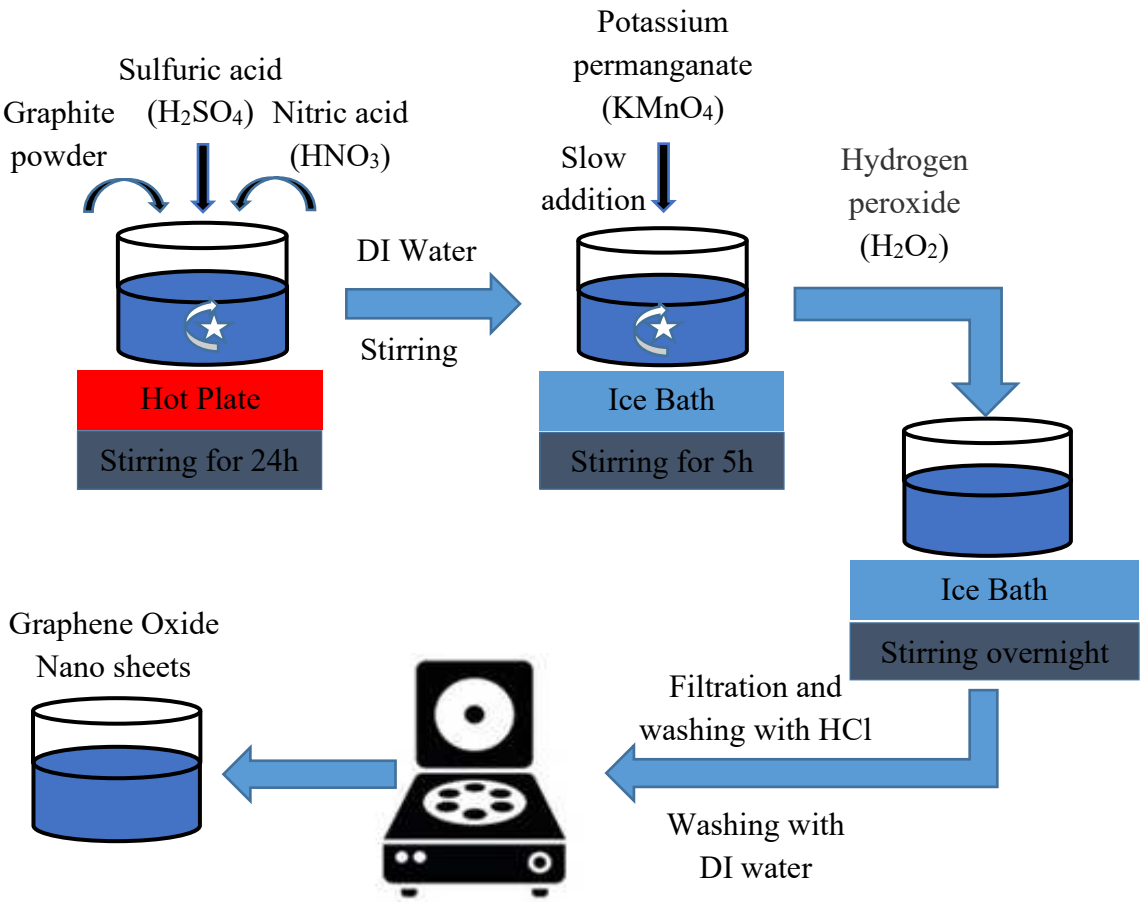
Sulfuric acid
Graphite powder
(H2SO4)
Nitric acid
(HNO3)
Potassium permanganate
(KMnO4)
Slow addition
Hydrogen peroxide
(H2O2)
DI Water
Stirring
Hot Plate
Stirring for 24h
Ice Bath
Stirring for 5h
Ice Bath
Stirring overnight
Filtration and washing with HCl
Washing with DI water
Graphene Oxide Nano sheets

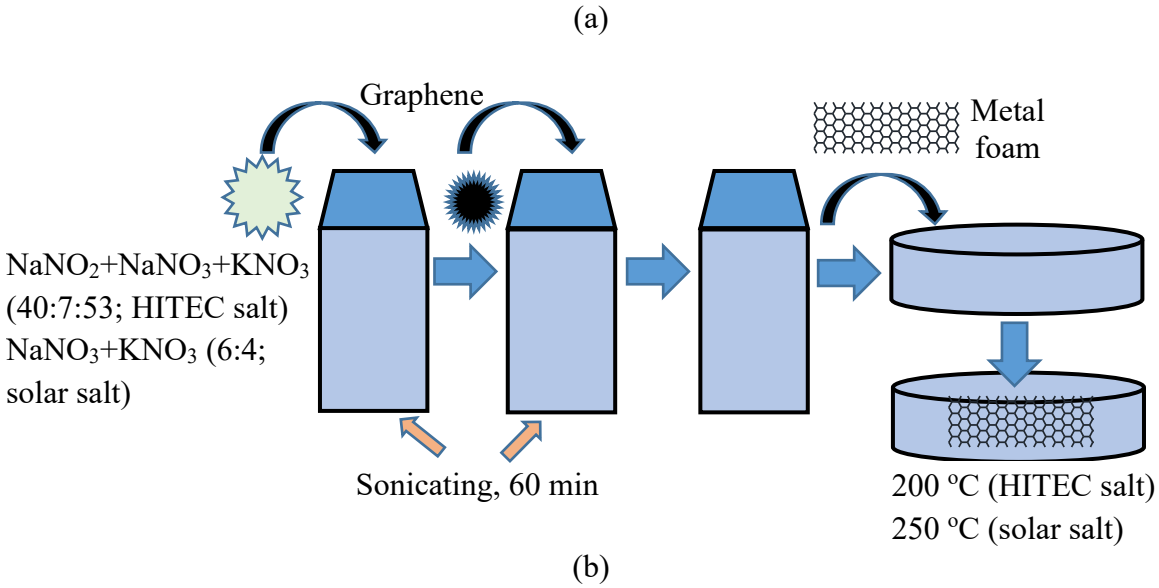

Figure 1. Schematic diagram of the synthesis processes. (a) graphene (b) salt/graphene/metal foam composites.

1

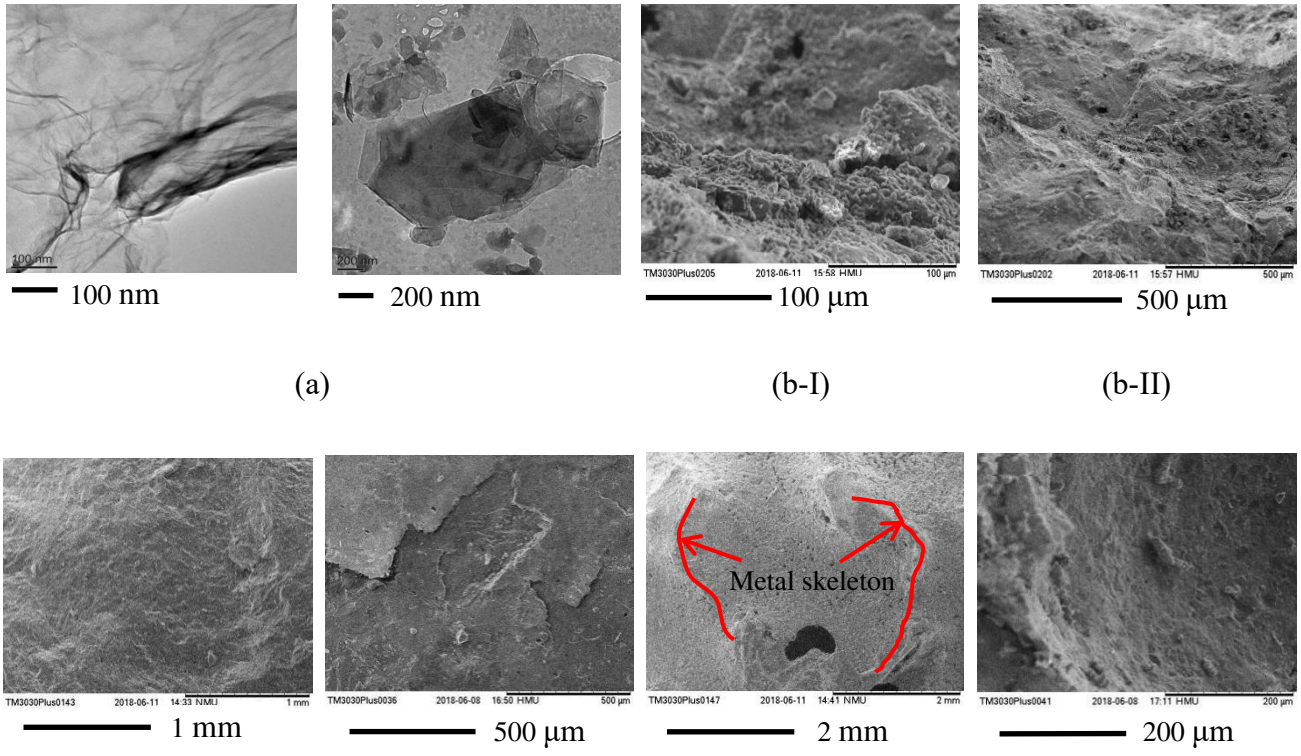

(c-I) (c-II) (d-I) (d-II)

Figure 2. TEM and SEM pictures of graphene (a), salt/3 wt.% graphene nanocomposites (b) salt/3 wt.% graphene/nickel foam composites (c) and salt/3 wt.% graphene/copper foam composites (d) (I: HITEC salt, II: solar salt).

1

2

3

4

5

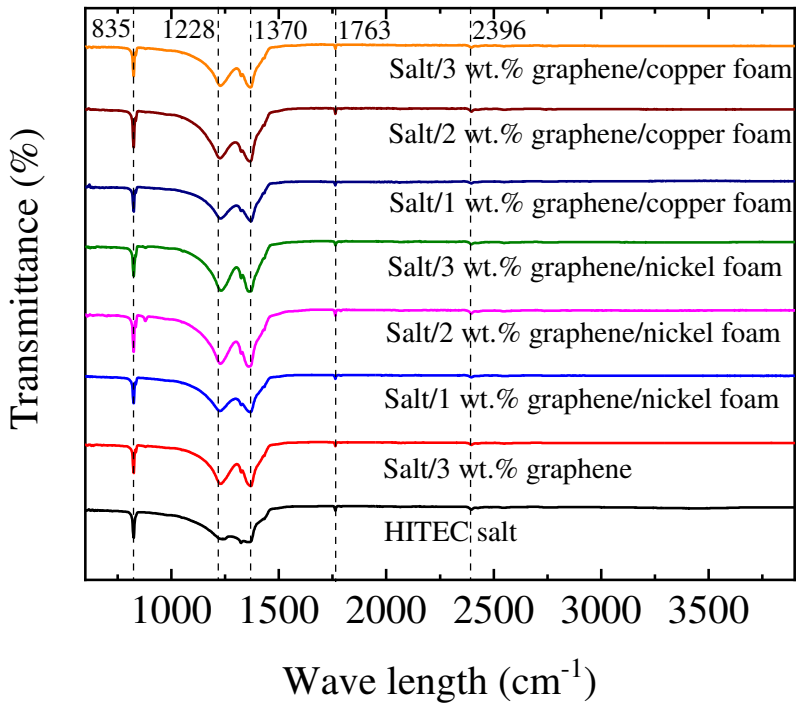

(a-I)

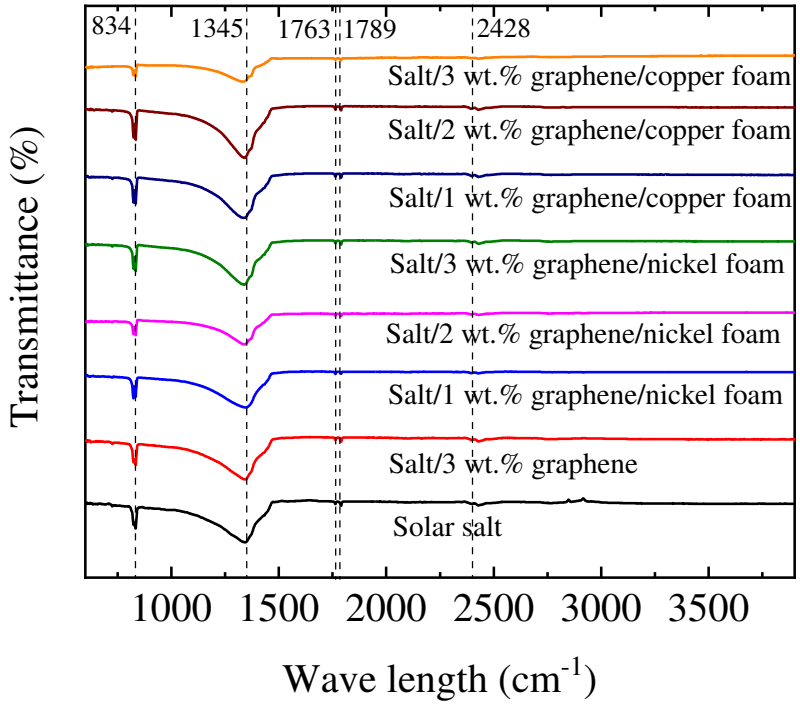
834
1345
1763
1789
2428
Salt/3 wt.% graphene/copper foam
Salt/2 wt.% graphene/copper foam
Salt/1 wt.% graphene/copper foam
Salt/3 wt.% graphene/nickel foam
Salt/2 wt.% graphene/nickel foam
Salt/1 wt.% graphene/nickel foam
Salt/3 wt.% graphene
Solar salt
Transmittance (%)
1000 1500 2000 2500 3000 3500
Wave length (cm-1)

(a-II)

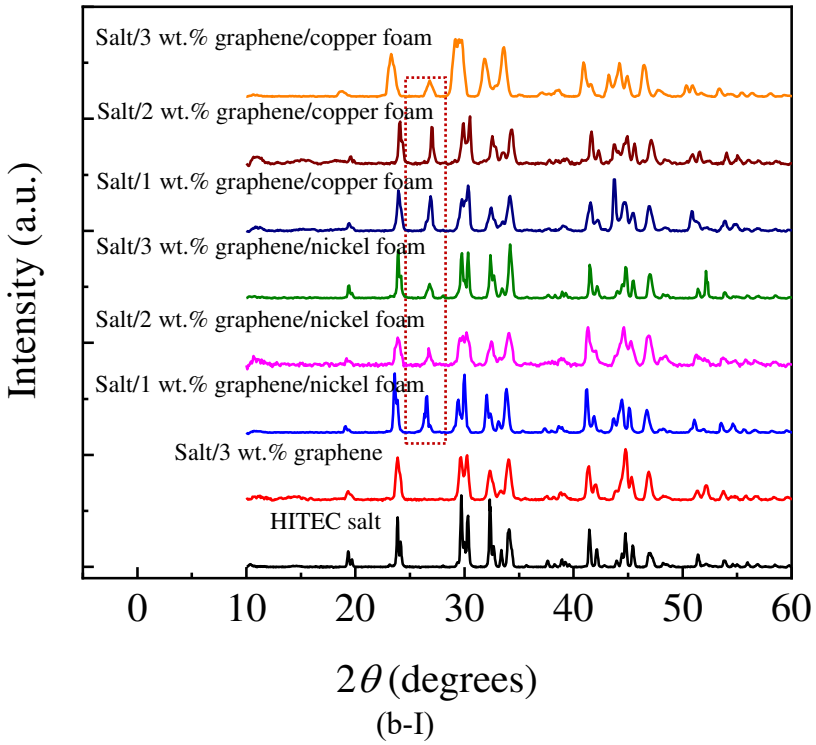
Salt/3 wt.% graphene/copper foam
Salt/2 wt.% graphene/copper foam
Salt/1 wt.% graphene/copper foam
Salt/3 wt.% graphene/nickel foam
Salt/2 wt.% graphene/nickel foam
Salt/1 wt.% graphene/nickel foam
Salt/3 wt.% graphene
HITEC salt
Intensity (a.u.)
0 10 20 30 40 50 60
2θ (degrees)

(b-I)

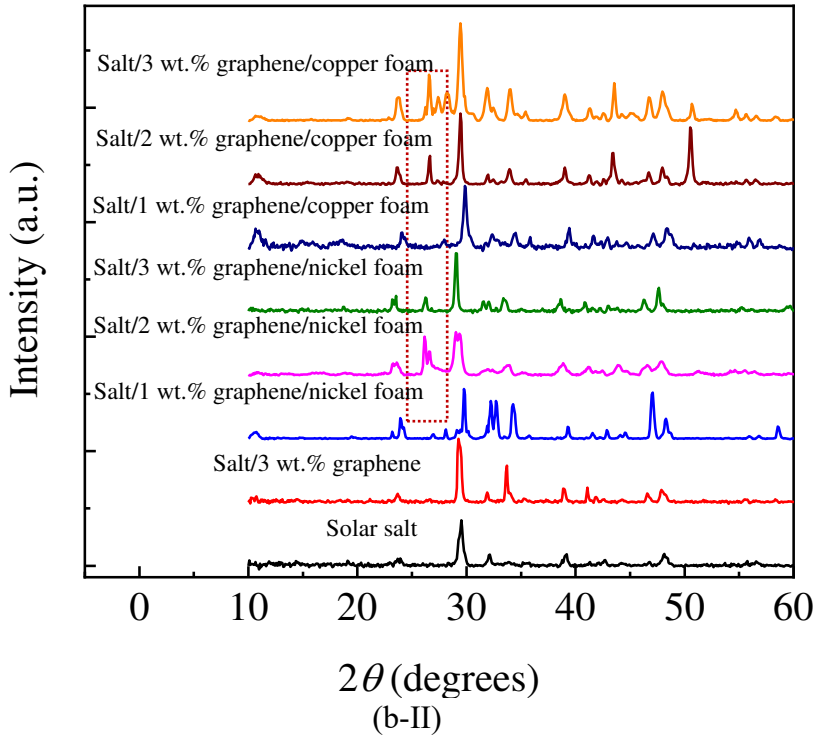

Figure 3. FT-IR (a) and XRD (b) curves of pure salt, salt/graphene nanocomposites and salt/graphene/metal foam composites. (I: HITEC salt, II: solar salt)

1

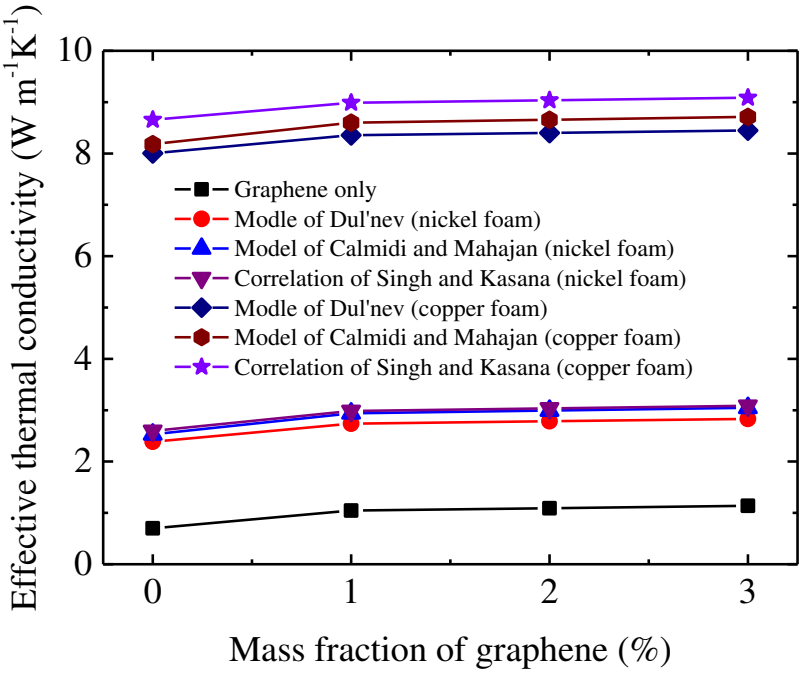

(a)

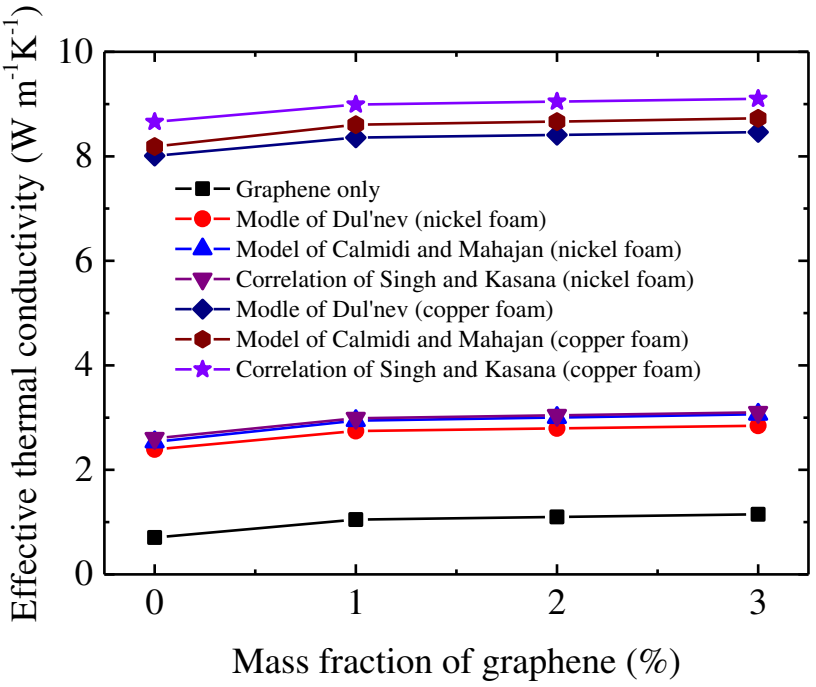

(b)

Figure 4. Effective thermal conductivities of salt/graphene nanocomposites and salt/graphene/metal foam composites. (a) HITEC salt (b) solar salt. (T=25 °C)

1

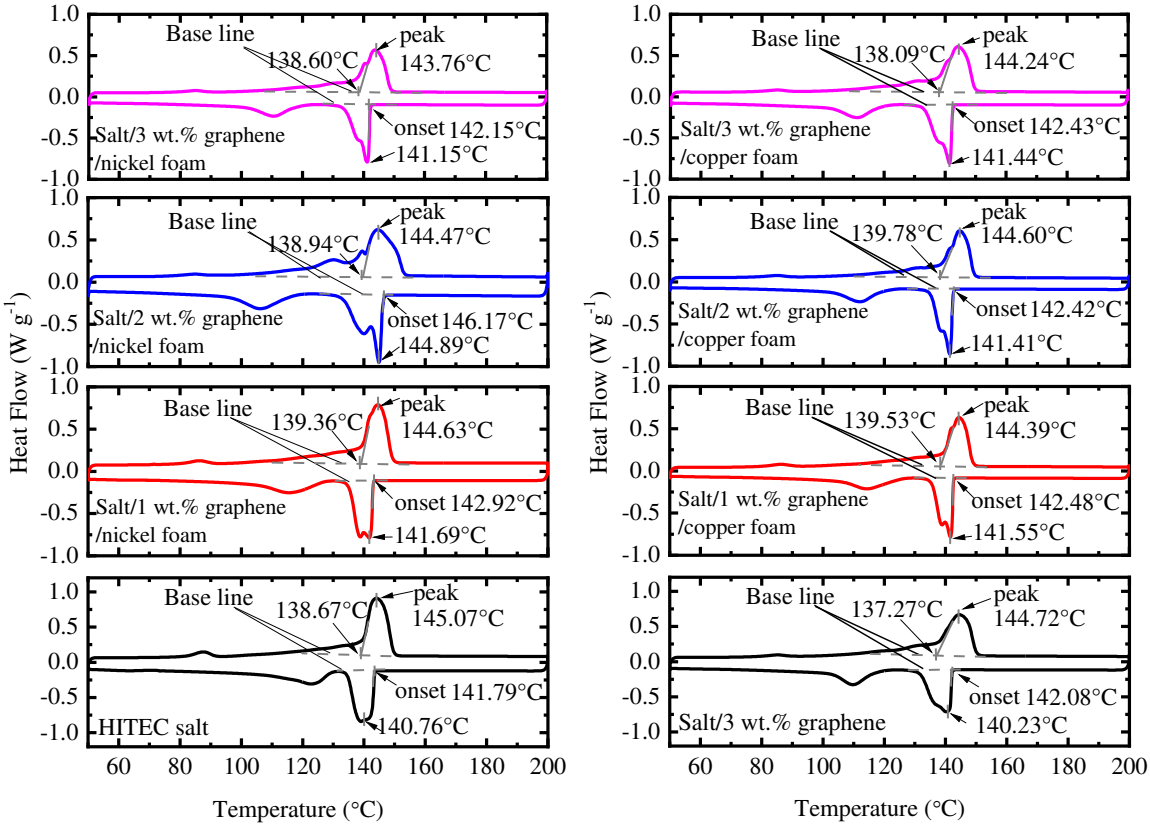
Heat Flow (W g-1)
Temperature (°C)
Base line
138.60°C
peak
143.76°C
onset 142.15°C
141.15°C
Salt/3 wt.% graphene
/nickel foam
Base line
138.94°C
peak
144.47°C
onset 146.17°C
144.89°C
Salt/2 wt.% graphene
/nickel foam
Base line
139.36°C
peak
144.63°C
onset 142.92°C
141.69°C
Salt/1 wt.% graphene
/nickel foam
Base line
138.67°C
peak
145.07°C
onset 141.79°C
140.76°C
HITEC salt
Base line
138.09°C
peak
144.24°C
onset 142.43°C
141.44°C
Salt/3 wt.% graphene
/copper foam
Base line
139.78°C
peak
144.60°C
onset 142.42°C
141.41°C
Salt/2 wt.% graphene
/copper foam
Base line
139.53°C
peak
144.39°C
onset 142.48°C
141.55°C
Salt/1 wt.% graphene
/copper foam
Base line
137.27°C
peak
144.72°C
onset 142.08°C
140.23°C
Salt/3 wt.% graphene

(a)

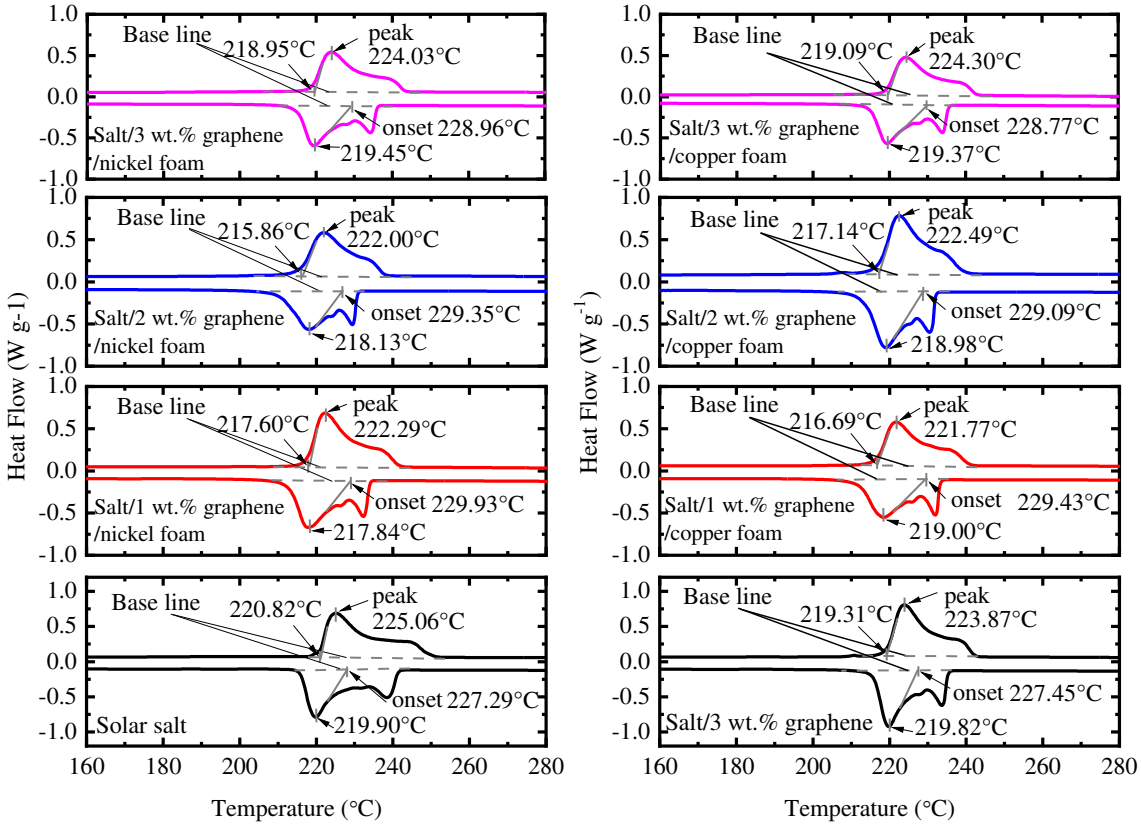

(b)

Figure 5. DSC curves of pure salt and salt/graphene/metal foam composites. (a) HITEC salt (b) solar salt.

1

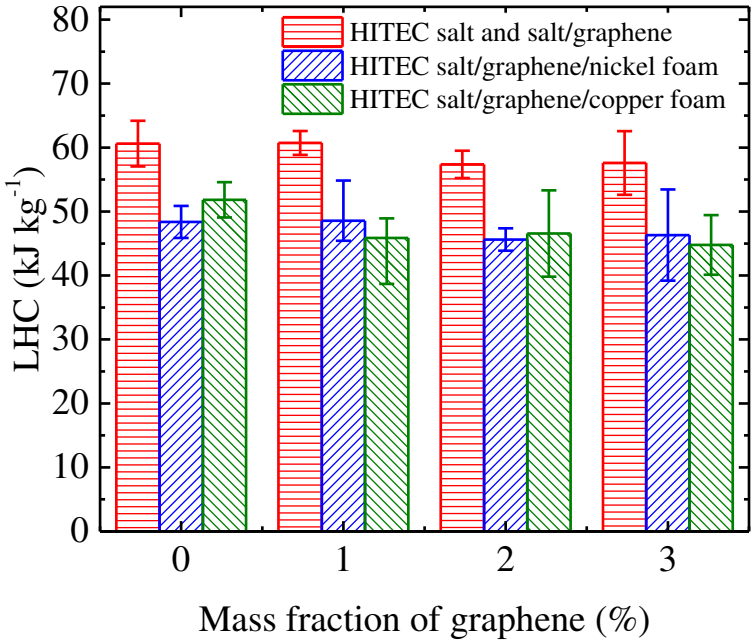

(a)

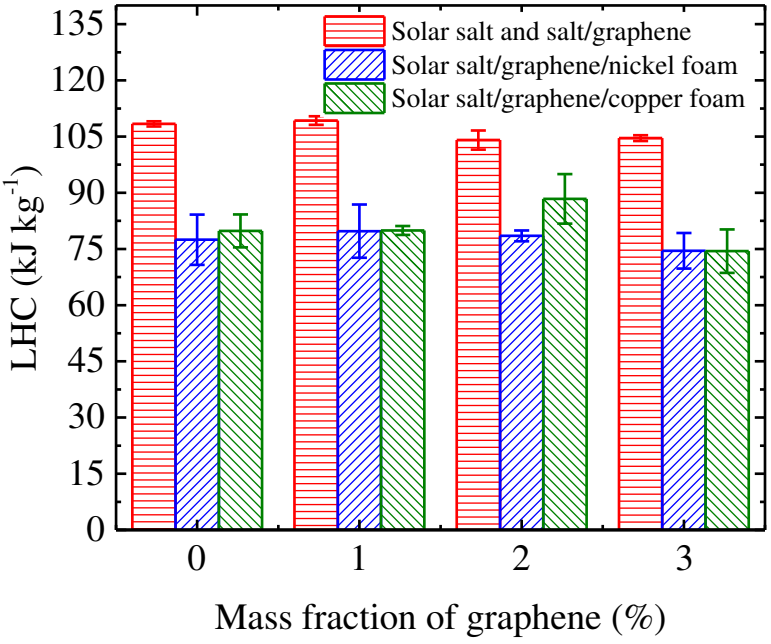

(b)

Figure 6. Comparison of latent heats for pure salt and salt/graphene/metal foam composites. (a) HITEC salt (b) solar salt.

1

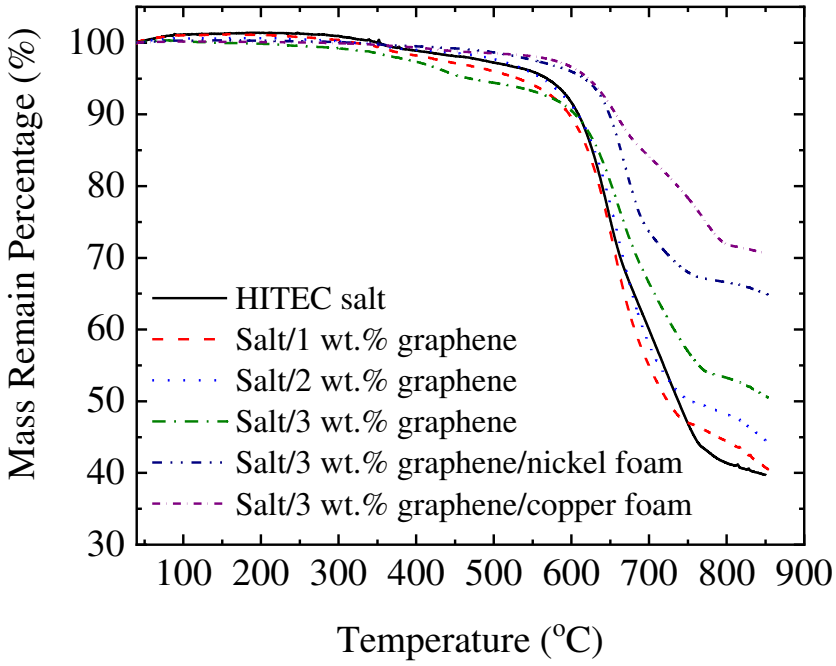

(a)

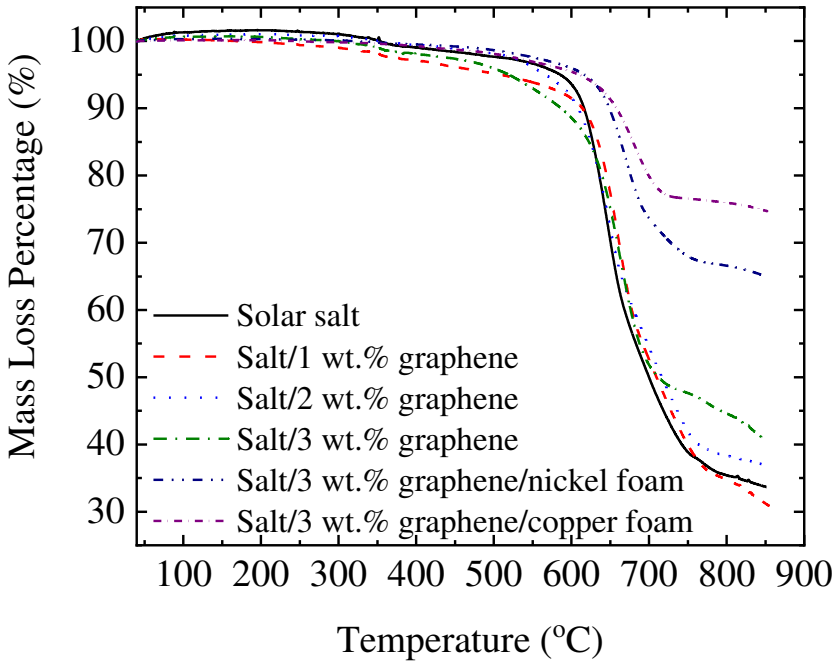

(b)

Figure 7. Thermo-gravimetric analyses of pure salt and salt/graphene/metal foam composites. (a) HITEC salt (b) solar salt.

2